ON THE HYDRODYNAMICS OF DYNAMIC STALL: AN EXPERIMENTAL STUDY

Thiago Fernandes Oliveira, thiagofernandesoliveira@gmail.com
Luciano Gonçalves Noleto, lucianonoleto@unb.br
Antonio C. P. Brasil Junior, brasiljr@unb.br
Universidade de Brasília, Faculdade de Tecnologia, Departamento de Engenharia Mecânica, Laboratório de Energia e Ambiente, 70910-900 - Asa Norte - Brasília, DF - Brasil

Abstract. *The objective of this work is the experimental study of a NACA 0018 airfoil in angular movement in a water tunnel. The lift, drag and pitching moment coefficients were measured statically and dynamically (along the airfoil's angular movement) through a load cell specifically designed for this study. The LabView software was used for the data acquisition and control of the experiment. The tests were performed for Reynolds numbers equal to 97,000, 124,000 and 150,000 for the statics cases and 124,000 and 150,000 for the dynamics cases with angular velocities of the airfoil equal to 0.01, 0.02 and 0.03 Hz. The results of the statics tests were compared with the literature with good agreement. The dynamic tests were performed to verify the phenomenon of dynamic stall. The results were compared between the different Reynolds numbers. The influence of the angular velocities in the dynamics cases was also evidenced comparing including with the static case. The flow visualization was also performed to complement the analysis.*

Keywords: *dynamic stall, NACA 0018, aerodynamic coefficients, load cell*

1. INTRODUCTION

The flow over moving boundaries holds great engineering interest. These flows are encountered in several areas, such as civil, mechanical, aerospace and biomechanical engineering. Traditional approaches are based on simplified methodologies that are customized to the problem. These methodologies have provided useful engineering tools (Naudascher and Rockwell, 2005). Dynamic stall is defined as the set of aerodynamical phenomena that happens as a consequence of airfoil angular movement. It happens due to an abrupt increase at the angle of attack (Ekaterinaris and Platzer, 1998; Fujisawa and Shibuya, 2001). Numerical and experimental works concerning this subject has the goal of measuring aerodynamical coefficients and flow topology (Larsen *et al.*, 2007). The literature also presents validation of numerical techniques that describes airfoil movement and dynamic stall prediction (Sahin *et al.*, 2003). One of the main dynamic stall characteristics is the drag and lift increase when compared with normal stall. One can find at the literature examples where the lift is twice the value in dynamic stall conditions (Shipley *et al.*, 1995). One can note a hysteretic behavior at lift, drag and moment coefficients. This behavior is due to the differences between inviscid and viscous timescales around the airfoil. These differences are physically defined by boundary layer separation delay, vortex formation at the leading edge of the airfoil, and vortex movement along the upper side of the airfoil (Divagalli, 1993; Ekaterinaris and Platzer, 1998).

The motivation behind the present work is the interest to investigate hydrodynamic phenomena linked to dynamic stall. Those phenomena are present on several flows, such as guide vanes of hydraulic turbines, helicopters and flapping wings. On the present work, the airfoil is moved with determined angular velocity from an initial to a final angle of attack. Aerodynamic coefficient measurement and flow visualizations were performed during airfoil movement until the final angle of attack is reached. Experimental runs were performed for several Reynolds values and for several angular velocities.

2. EXPERIMENT DESCRIPTION

2.1 Water Tunnel

The present work was performed at a Armfield water tunnel model HAN 5, with 2750 mm of height, 4900 mm of length and 1100 mm width, utilizing a pump with 5.500 W of nominal power. The schematics and photo of the water tunnel are shown at figure 1:

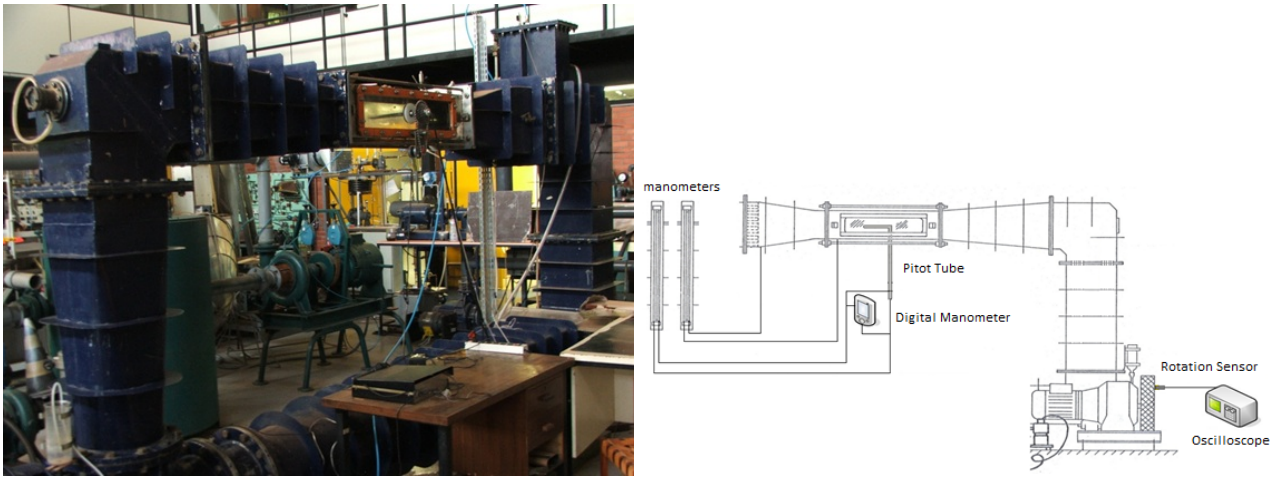

Figure 1. Water Tunnel

The activation and control of the pump are made by a frequency converter, which executes velocity variation. The test section is formed by a square section area of 200 mm of height and width and 750 mm length. Inside this section, flow velocity can reach from 0,65 to 4,8 m/s. The turbulence intensity of the tunnel is below 0.2% . The test section also has two acrilic walls at its sides and one at the bottom, allowing flow visualization. An aluminum NACA 0018 airfoil with 89 mm of chord and 198 mm of span was used for the experiences. The airfoil is solid and drilled at $1/4$ of the chord from the leading edge for the spinning axis. In this section, a weight system coupled to an airfoil is positioned as shown in figure 2:

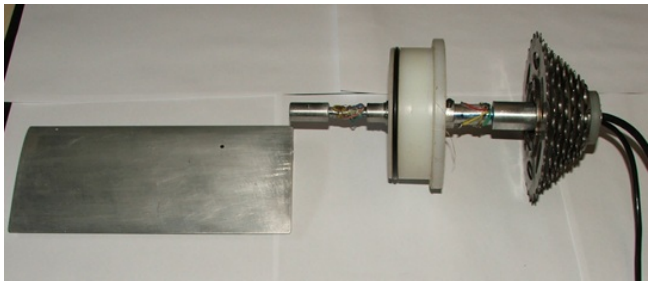

Figure 2. Airfoil and moving system

The airfoil is moved by a stepper motor who has a resolution of 1.8 degrees per step. The motor was connected to a control driver that has a half-step option, which is used in all experimental runs. The position and angular velocity of the airfoil were defined and controlled by an *LabView* algorithm. The transmission between the stepper motor and the spinning axis of the airfoil, which contains a load cell was made by a pinion-Derailleur gear reduction with chains (figure 3). The reduction was employed to obtain torque enhancement and better resolution of airfoil positioning. The pinion was coupled directly to the stepper motor axis and has 33 mm of diameter. The Derailleur gear was directly coupled to the load cell and the spinning axis of the airfoil with 99 mm of diameter. A 3:1 reduction was obtained by this gear system. The half-step option and the used reduction allowed a angular positioning reduction of 0.3 degrees.

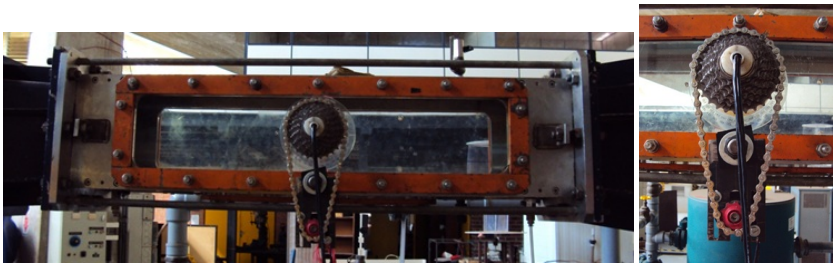

Figure 3. Water Tunnel

2.2 Instrumentation

Two methodologies were used to measure flow velocity. The first method employed a Pitot tube connected to a differential fluid-column manometer and a digital differential manometer. The second method measured the pressure variation between the inlet and outlet of the nozzle of the test section. Here, pressure measurements were performed by another differential fluid-column manometer.

The load cell was divided into two sections. The first one measures the drag and lift forces inside the airfoil. The other measures the torque caused by the momentum. Two unidirectional extensometers were employed for drag and lift measurements each, forming two half-Wheatstone bridges that measures each force. The third is a full-Wheatstone bridge is used to measure momentum. Its schematics are shown in figure 4:

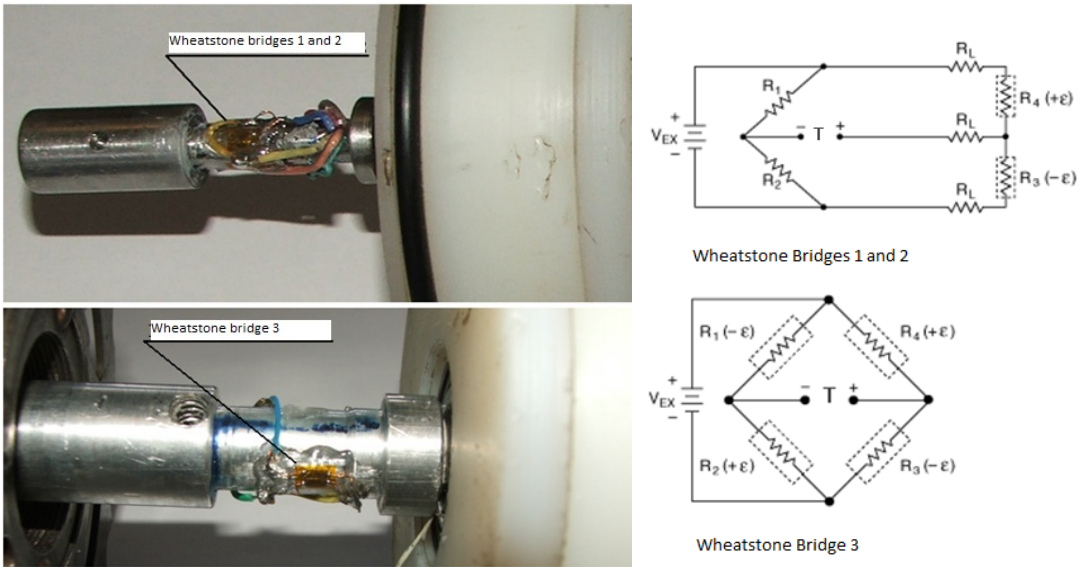

Figure 4. Load cell and Wheatstone bridges

The data acquisition system is a NI cDAQ-9172 rack. Its two modules were employed for extensometry acquisition and pressure and rotation measurement respectively. The stepper motor control was performed by a control driver with serial communication, linked directly to a computer by a USB cable. The *LabView* software was employed for data acquisition and treatment and movement control of the airfoil. This system allows the dynamic acquisition of:

- Flow velocity by acquisition of pressure and rotation data;
- Airfoil loads with extensometry;

The automatic acquisition of those data, conjugated by the movement control of the airfoil, allowed the measurement of dynamic loads during airfoil movement. Flow visualization was performed to a better comprehension of the dynamic stall phenomena. A CANON photographic camera, with a SONY video camera and a diode laser was used for this visualization. The laser is responsible for creating a light plane that illuminates pliolite particles inside the flow. Those particles has good light reflexive properties. The cameras were positioned at a perpendicular position for image acquisition (figure 5).

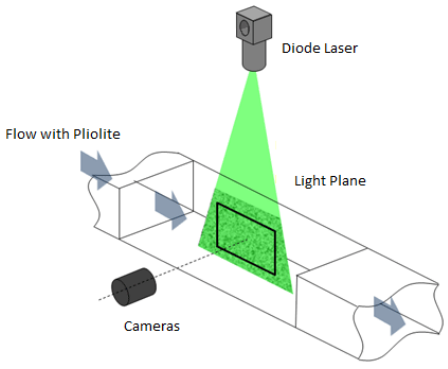

Figure 5. Load cell and Wheatstone Bridges

2.3 Methodologies and Data Treatment

Four experimental runs were performed for this article:

- Water tunnel calibration;
- Load cell calibration;
- Acquisition of the aerodynamic coefficients;
- Flow Visualization;

The water tunnel was calibrated to obtain the average velocity and velocity profile at the test section as a function of the rotation of the main pump. The Pitot tube was coupled to a differential manometer, with a digital manometer to obtain the dynamic pressure and flow velocity. For pump rotation measurement, a inductive proximity sensor was employed as a rotation sensor at the pulley coupled at the pump. With that, flow velocity was varied on-the-fly at the experimental run. The calibration procedure was performed by the following *rationale*:

- For a fixed rotation, dynamic pressure data were obtained;
- Velocity calculation by the Bernoulli equation;
- Velocity Coupling with each rotation;

A NACA 0018 symmetric profile was employed at the experimental run. The first part contemplate the static runs, where the airfoil was fixed on the following angles: 0.0, 0.9, 1.9, 3.1, 4.0, 5.0, 5.9, 6.9, 8.1, 9.0, 10.0, 10.9, 12.1, 13.1, 14.0, 15.0, 15.9, 17.1, 18.1, 19.0 and 19.9. Here, the objective was the load cell methodology validation, where the static coefficients were compared with the literature. On the second part, the dynamic runs were performed, where the coefficients were calculated on-the-fly during the airfoil movement. Those runs were performed for two Reynolds numbers and three angular velocities. In all runs, the attack angle was varied from 0 to 19.8.

At the first part, the Reynolds numbers were equal to 97.000, 124.000 e 150.000, respectively. The used angular velocities were 0.01, 0.02 e 0.03 Hz. All the runs, static and dynamic, were repeated five times to obtain a ensemble average. Flow visualization were performed for both runs at a Reynolds number of 150.000 with the same angular velocities. Certain angles were conveniently chosen for visualization an analysis. All data were acquired with a continuous 2 Hz rate, with a buffer size equal to 2048. Fourth-order Bessel low-pass filters were employed, with a cut-off frequency of 12 Hz. Those configurations allowed an adequate acquisition rate and a short system response time, avoiding synchronizing problems between measured loads and profile positioning during the dynamic runs. All bridges were balanced at $\alpha = 0$. The hydrodynamic forces were obtained by the load cell with the following equations:

$$\overrightarrow{F_1} = K_1 T_1 \tag{1}$$
$$\overrightarrow{F_2} = K_2 T_2 \tag{2}$$
$$\overrightarrow{M} = K_3 T_3 \tag{3}$$
$$\overrightarrow{W_{ap}} = \overrightarrow{W} + \overrightarrow{E} \tag{4}$$

The Wheatstone bridges calibration yielded the following proportionality coefficients: $K_1 = 125.319$, $K_2 = 102.947$ e $K_3 = 12.227$. T is the milivoltage sign by extensometers out. W_{ap} is the apparent weight of the airfoil. Clockwise movement was imposed as a convention for positive yawing momentum. The lift, drag, momentum and the attack angle were obtained as follows:

$$\mid L \mid = \mid F_1 \mid cos(\alpha) + \mid F_2 \mid sin(\alpha) + \mid W_{ap} \mid cos(\alpha) - \mid W_{ap} \mid \tag{5}$$

$$\mid D \mid = \mid F_2 \mid cos(\alpha) + \mid F_1 \mid sin(\alpha) + \mid W_{ap} \mid sin(\alpha) \tag{6}$$

$$\mid M \mid = \mid D' \mid cos(\alpha) + \frac{3}{4} c \mid W_{ap} \mid sin(\alpha) \tag{7}$$

$$\alpha = \omega t \tag{8}$$

Where c is the chord of the airfoil. One must consider that the load cell turns with the airfoil. With the hydrodynamic forces and momentum, the coefficients were given as follows:

$$C_L = \frac{L}{0.5 \rho_{H2O} A_p U^2} \tag{9}$$

$$C_D = \frac{D}{0.5\rho_{H2O}A_pU^2} \tag{10}$$

$$C_M = \frac{M}{0.5\rho_{H2O}A_pU^2c} \tag{11}$$

With:

$$A_p = c \times e \tag{12}$$

Flow velocity during the experimental runs were estimated by the frequency of the converter, given as follows:

$$U = 0.0037f \tag{13}$$

The frequency was also monitored at the pump with the following equation:

$$U = 0.0064f_{pump} \tag{14}$$

3. RESULTS AND DISCUSSION

All data presented at the curves on this article uses an arithmetic averaging of five experimental runs for each configuration, in order to make an uncertainty analysis for the experiments.

3.1 Static Case

Figure 6 shows the results for the static runs. One can observe that the lift coefficient behavior presents little variation with the Reynolds number. This result was expected, because all the Reynolds numbers has the same order. The maximum value for lift is 0.9 for an angle of 10.9 degrees and Reynolds equal to 97000. For the remaining Reynolds, one can obtain maximum lift around 1 for an angle of 12.1 degrees. The drag coefficient results shown similarity between the three studied Reynolds. The momentum coefficient presented different behaviors for each Reynolds. One can note also an important fluctuation on those values with the angle of attack. Figure 7 compares the obtained results with the results of (Timmer, 2008). This comparison has the objective of validation of the results and the load cell. Figure 7(c) show the lift results. The results of this article present good agreement with the reference when one compares maximum lift, stall angle and curve behavior pre and post stall. Figure 7(a) compares the drag data. As before, a good agreement is obtained, specially at the pre-stall region. Little difference is noted at the post-stall values. Figure 7(d) compares the momentum data, and as the previous, the obtained results are in good agreement. One can conclude that the load cell is working adequately and the employed methodology is giving good results for the aerodynamic coefficients.

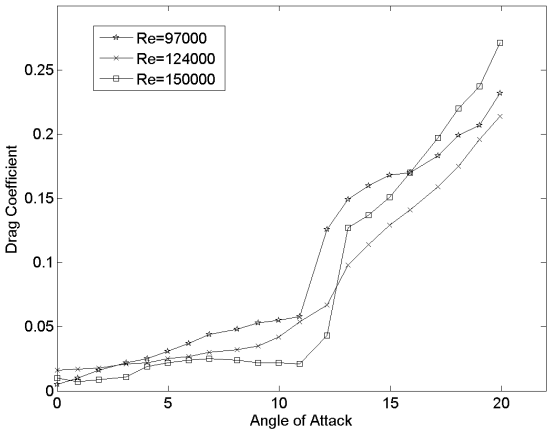

(a) Drag Coefficient

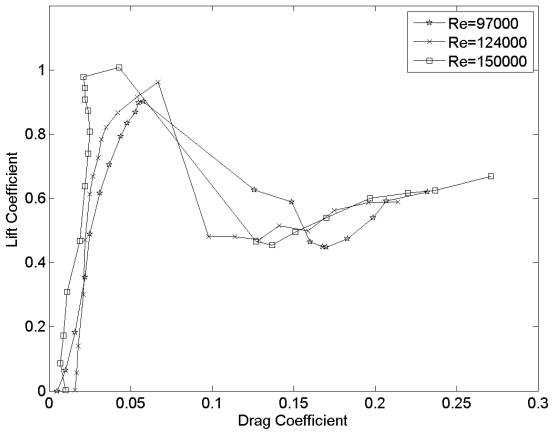

(b) Drag Polar

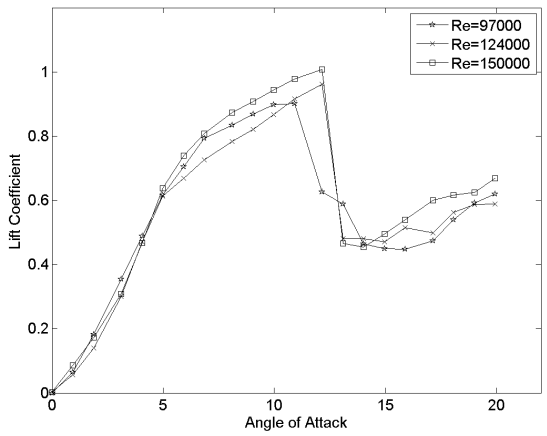

(c) Lift Coefficient

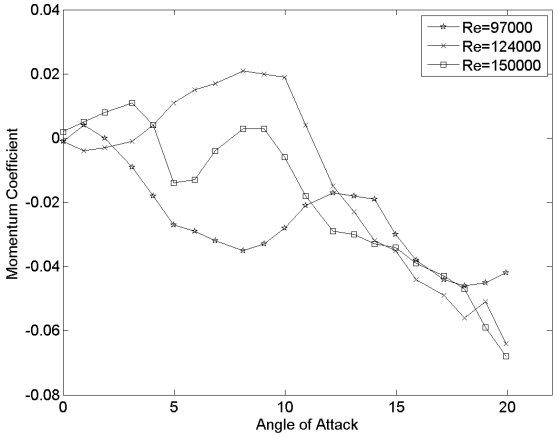

(d) Momentum Coefficient

Figure 6. Aerodynamic Coefficients - Static Case

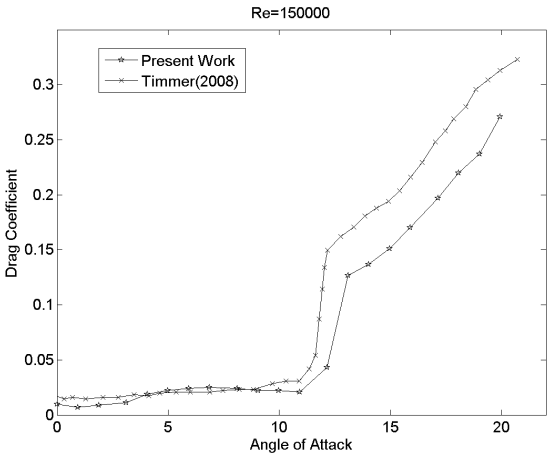

(a) Drag Coefficient

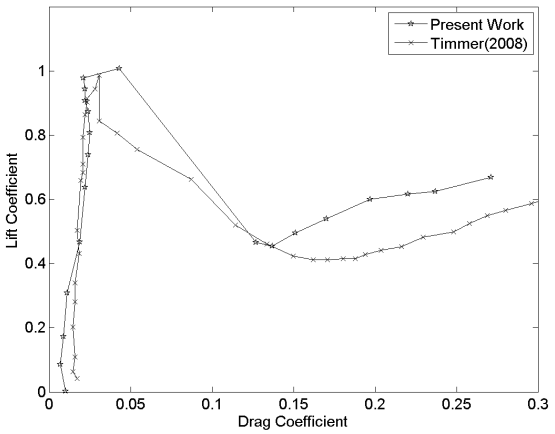

(b) Drag Polar

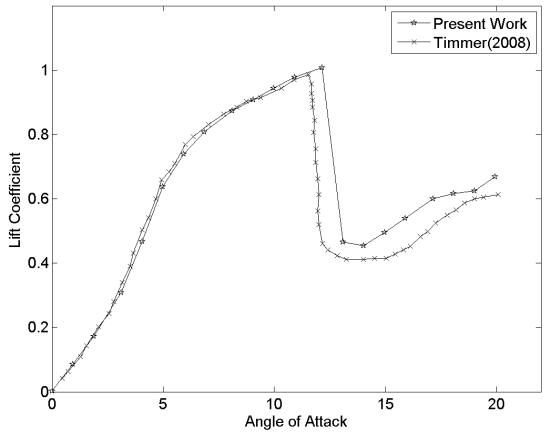

(c) Lift Coefficient

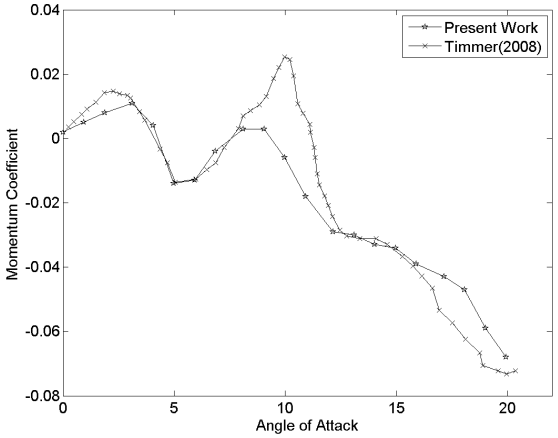

(d) Momentum Coefficient

Figure 7. Data Comparing - Re=150000

Figure 8(a) show the airfoil at zero degrees. One can note that the flow develops without boundary layer detachment, as expected for this angle. The lift and moment coefficient are equal to zero, as expected for symmetric airfoils. Drag

results are close to zero on this angle, where little drag is obtained due to viscous drag. Figure 8(b) presents the airfoil at 13.1 degrees. The flow does not present detachment patterns yet. On this angle, viscous drag are the bigger contributor for overall drag obtained. Figure 8(c) show the airfoil at a angle of 15.9 degrees. One can note a recirculation zone at the trailing edge. A considerable drag increase is noted on this angle, as well as a loss in lift. Momentum results are around -0.07. For the angle of 19.9 (figure 8(d)), the recirculation zone at the trailing edge has degenerated to a vortex wake. One can note that the leading edge has a clear recirculation zone. Also, one can note temporal variation at all coefficients. At this angle, drag has a major contribution of pressure drag.

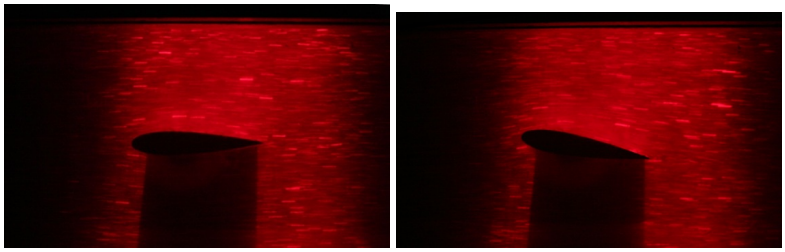

(a) Zero Degrees (b) 13.1 Degrees

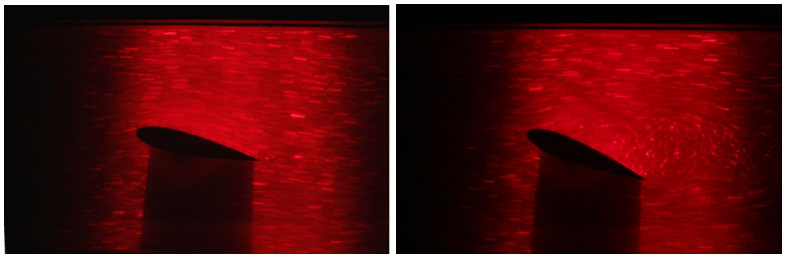

(c) 15.9 Degrees (d) 19.8 Degrees

Figure 8. Flow Visualization - Static Case

3.2 Dynamic Case

Figure 9 shows the lift coefficient curves for three angular velocities of the airfoil: 0,01, 0,02 e 0,03 Hz for Reynolds numbers of 124.000 e 150.000. One can note that the maximum lift obtained is equal to 1.35 for a angle of 17.6 degrees, angular velocity equal to 0.03 and Reynolds of 124.000. Drag and momentum behavior for this situation is presented by figures 9(a) to 9(l). The momentum coefficient presented an oscillating behavior during the airfoil movement. All coefficients presented sensitivity to Reynolds number variation. When one compares the static and dynamic results for all coefficients, it is noted the angular velocity influence at the results. It is also noted the stall delay at the dynamic cases when compared with the static cases, as well as the lift increase. This increase is about 25 to 35% of the static values. For a Reynolds number of 150.000, one can note the sensitivity mentioned before. The static and dynamic cases are more distinct between each other. It is observed the stall delay and the lift increase, which is about 7 and 22%. Drag results also show the stall delay at the dynamic results. It is noted for both Reynolds that the drag has little sensitivity to the angular velocity. Momentum results, on the other hand, has more sensitivity.

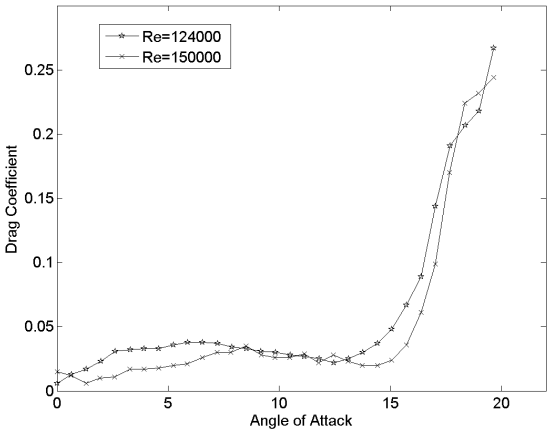

(a) Drag Coefficient for $\omega = 0.01$

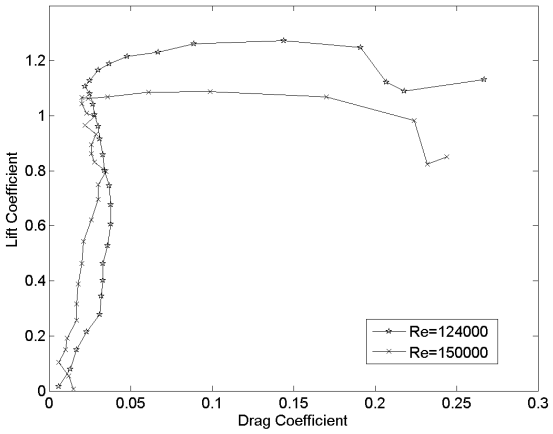

(b) Drag Polar for $\omega = 0.01$

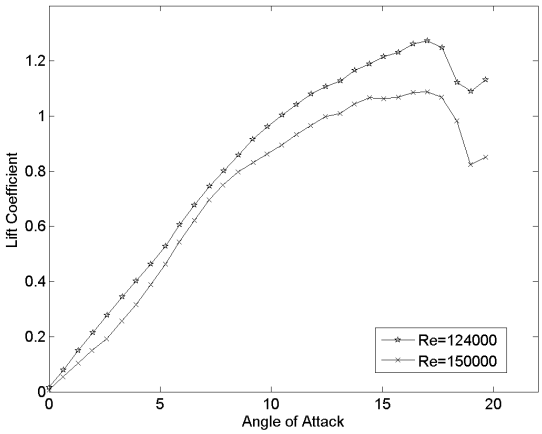

(c) Lift Coefficient for $\omega = 0.01$

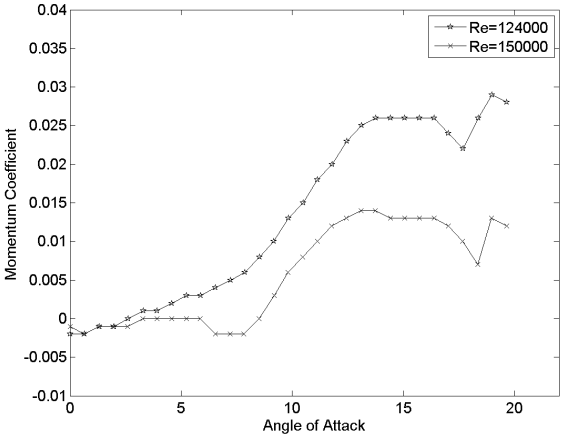

(d) Momentum Coefficient for $\omega = 0.01$

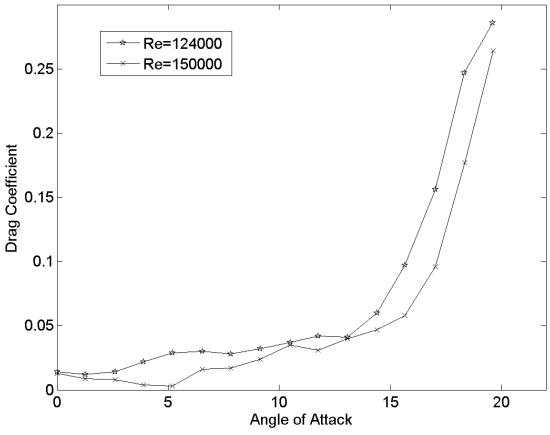

(e) Drag Coefficient for $\omega = 0.02$

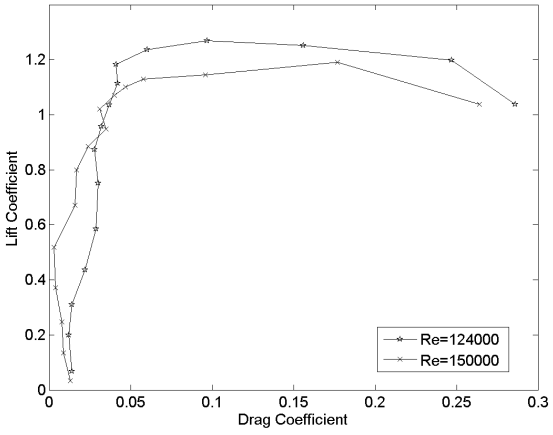

(f) Drag Polar for $\omega = 0.02$

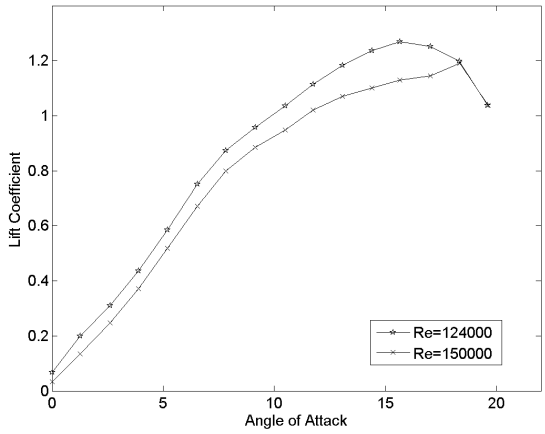

(g) Lift Coefficient for $\omega = 0.02$

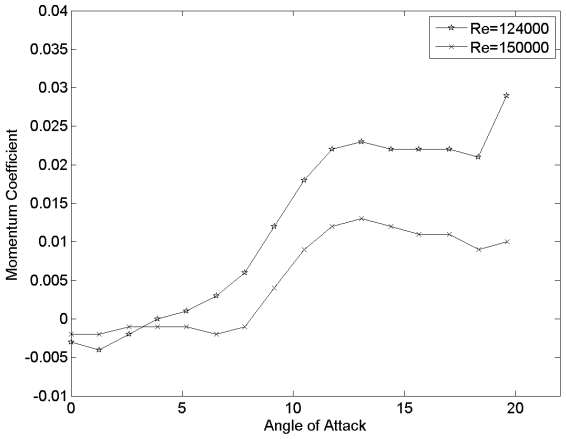

(h) Momentum Coefficient for $\omega = 0.02$

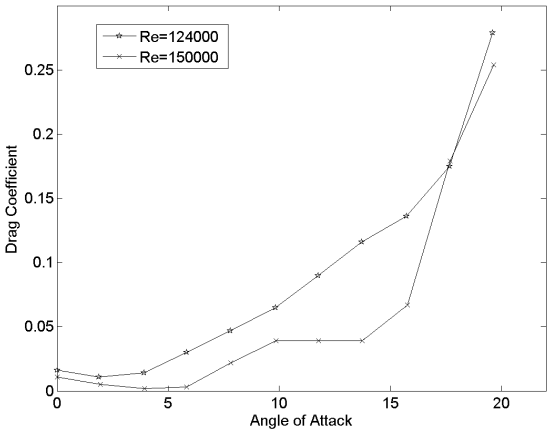

(i) Drag Coefficient for $\omega = 0.03$

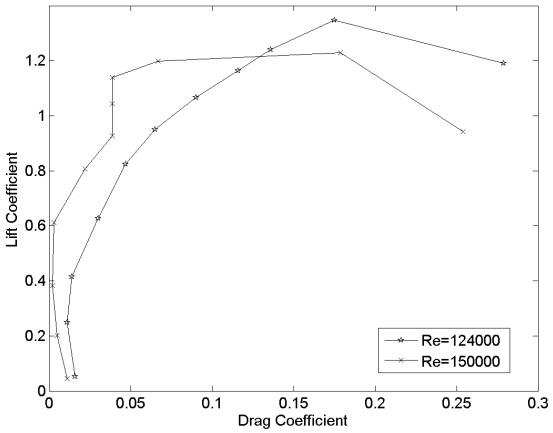

(j) Drag Polar for $\omega = 0.03$

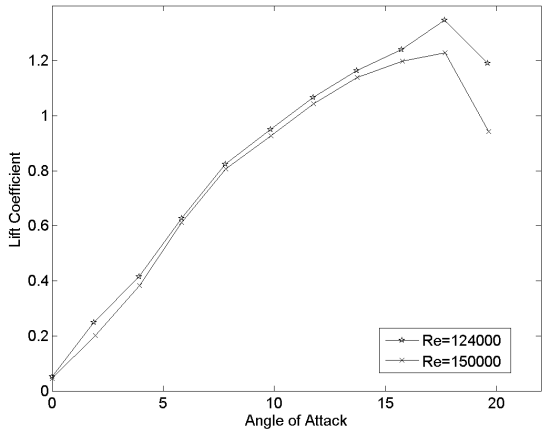

(k) Lift Coefficient for $\omega = 0.03$

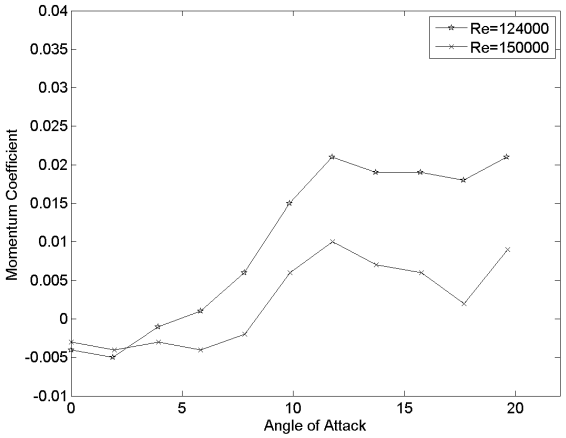

(l) Momentum Coefficient for $\omega = 0.03$

Figure 9. Aerodynamic Coefficients - Dynamic Case

Figure 10 show the profile at 0, 10, 14 and 19 degrees of angle of attack respectively for a Reynolds number of 150.000 and angular velocity of 0.01 Hz. The static case shows signs of boundary layer detachment at 13 degrees, while on the dynamic case, this angle does not present any detachment signs. Those signs appears at 14 degrees. At 17 degrees, one can observe the formation of small recirculation zones at the trailing edge. At 19 degrees, the first signs of detachment and degeneration to a vortex wake begins to appear. The visualizations of this case showcases the dynamic stall behavior.

Stall delay, lift peak and drag behavior are noted at the aerodynamic coefficients, and these effects are confirmed by the flow behavior at the airfoil.

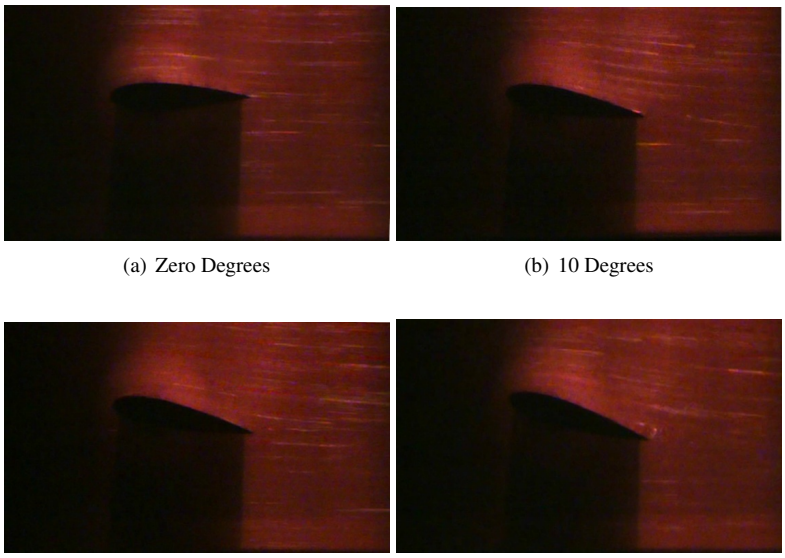

(a) Zero Degrees (b) 10 Degrees

(c) 14 Degrees (d) 19 Degrees

Figure 10. Flow Visualization - Dynamic Case

4. CONCLUSIONS

The present paper performed experimental runs to obtain lift, drag and momentum coefficients of a NACA 0018 profile for dynamic stall analysis. Those coefficients were obtained with a experimental setup developed specifically for this study. Static and dynamic runs were performed for three chord-based Reynolds numbers. The results were compared with the literature to validate the results.

The most significant result were the comparison between static and dynamic data for the same Reynolds number. One can observe significant increase, around 20% at the lift. It is also noted the stall delay. The static case has its stall at 12 degrees and the dynamic case has its stall at 17 degrees. These results represents well the dynamic stall influence at the behavior of the aerodynamic coefficients and the acting forces on the airfoil. The flow visualization had a more qualitative aspect. One can note the dynamic stall effects on the flow topology, observing the boundary layer detachment patterns and when those patterns appears.

Concluding, this experimentation has produced results that showcases the main aspects of dynamic stall. For a better understand of all the phenomena linked to this kind of stall, more Reynolds numbers need to be studied. Also, the use of modern techniques of flow visualization, such as PIV or LIF can also give more information of the velocity field.

5. REFERENCES

Divagalli, S.K., 1993. *Dynamic Stall of a NACA 0012 Airfoil in Laminar Flow*. Ph.D. thesis, Massachussetts Institute of Technology.

Ekaterinaris, J. and Platzer, M., 1998. "Computational prediction of airfoil dynamic stall". *Progress in Aerospace Sciences*, Vol. 33, No. 11-12, pp. 759–846.

Fujisawa, N. and Shibuya, S., 2001. "Observations of dynamic stall on turbine blades". *Journal of Wind Engineering and Industrial Aerodynamics*, Vol. 89, No. 2, pp. 201–214.

Larsen, J., Nielsen, S. and Krenk, S., 2007. "Dynamic stall model for wind turbine airfoils". *Journal of Fluids and Structures*, Vol. 23, No. 7, pp. 959–982.

Naudascher, E. and Rockwell, D., 2005. *Flow Induced Vibrations: An Engineering Guide*.

Sahin, M., Sankar, L.N., Chandrasekhara, M.S. and Tung, C., 2003. "Dynamic stall alleviation using a deformable leading edge concept - a numerical study". *Journal of Aircraft*, Vol. 40, No. 1, pp. 77–85.

Shipley, D.E., Miller, M.S. and Robinson, M.C., 1995. "Dynamic stall occurrence on a horizontal axis wind turbine blade". Vol. 16, pp. 167–173.

Timmer, W., 2008. "Two-dimensional low-reynolds number wind tunnel results for airfoil naca 0018". Technical report, Wind Energy Section, Faculty of Aerospace Engineering, Delft University of Technology, Kluyverweg 1, Netherlands.